AIP | Journal of Applied Physics

Local impedance measurement of an electrode/single-pentacene-grain interface by frequency-modulation scanning impedance microscopy

Tomoharu Kimura, Kei Kobayashi, and Hirofumi Yamada

Citation: Journal of Applied Physics **118**, 055501 (2015); doi: 10.1063/1.4927921
View online: http://dx.doi.org/10.1063/1.4927921
View Table of Contents: http://scitation.aip.org/content/aip/journal/jap/118/5?ver=pdfcov
Published by the AIP Publishing

Local impedance measurement of an electrode/single-pentacene-grain interface by frequency-modulation scanning impedance microscopy

Tomoharu Kimura,[1] Kei Kobayashi,[1,2] and Hirofumi Yamada[1,a)]
[1]*Department of Electronic Science and Engineering, Kyoto University, Kyoto 615-8510, Japan*
[2]*The Hakubi Center for Advanced Research, Kyoto University, Kyoto 615-8520, Japan*

(Received 20 April 2015; accepted 17 July 2015; published online 5 August 2015)

The device performances of organic thin film transistors are often limited by the metal–organic interface because of the disordered molecular layers at the interface and the energy barriers against the carrier injection. It is important to study the local impedance at the interface without being affected by the interface morphology. We combined frequency modulation atomic force microscopy with scanning impedance microscopy (SIM) to sensitively measure the ac responses of the interface to an ac voltage applied across the interface and the dc potential drop at the interface. By using the frequency-modulation SIM (FM-SIM) technique, we characterized the interface impedance of a Pt electrode and a single pentacene grain as a parallel circuit of a contact resistance and a capacitance. We found that the reduction of the contact resistance was caused by the reduction of the energy level mismatch at the interface by the FM-SIM measurements, demonstrating the usefulness of the FM-SIM technique for investigation of the local interface impedance without being affected by its morphology. © *2015 AIP Publishing LLC*.
[http://dx.doi.org/10.1063/1.4927921]

I. INTRODUCTION

Organic electronics have currently attracted many researchers' attention because of their potential applications to light-weight and flexible electronic devices by simple and cost-effective fabrication processes.[1,2] The performances of organic field-effect transistors (OFETs), which are one of the basic devices in organic electronics, are still not sufficient for practical applications. For example, the charge transport in the OFETs is often limited not only by the intrinsic characteristics of the organic thin films but also by the electronic properties at the metal–organic interfaces.[3,4] The influence of the electronic properties of the metal–organic interface becomes even noticeable for the OFETs with a short channel length and those using the organic molecule exhibiting a high carrier mobility.[5,6] In order to overcome the limitation of the device performances, more intensive research focused on the metal–organic interfacial properties is becoming important.

The metal–organic interface often exhibits an electrical contact resistance. It has been well known that the contact resistances in the OFETs often show non-linear current-voltage characteristics[6,7] and also depend on the gate bias voltages,[8–10] which makes it difficult to control the device performances. An energy level mismatch at the metal–organic interfaces is thought to be one of the origins of the contact resistance; a difference between the Fermi energy (E_F) of the metal and the highest occupied molecular orbital (HOMO) energy of the organic film (E_{HOMO}) induces a hole injection barrier for hole conducting materials. For example, Bürgi *et al.*[11] found a large contact resistance at the metal–organic interface when they used a metal with a small work function for the electrode, and other reports showed the reduction of the contact resistance by modifying the electrode with self-assembled monolayers (SAMs)[12,13] or thin metal-oxide layers.[14] Wang *et al.*,[9,15] however, suggested another possible reason for the contact resistance and its gate-bias dependence that the mobility of the disordered organic thin films near the metal electrodes becomes low and the disordered film area works as a contact resistance. These previous studies imply that the metal–organic interface properties are extremely complex, and the origin of the contact resistances and its gate-bias dependence is still under discussion.

The impedance of the metal–organic interfaces has been studied by various impedance measurement techniques, such as the transition line method,[16] capacitance–voltage measurement,[17] and impedance spectroscopy.[18] By using these techniques, we can measure the dependence of the contact resistance and metal–organic capacitance on the gate bias voltage and obtain information on the energy levels and densities of the traps. However, these electrical measurements require large-area electrodes; thereby, the measured impedance is inherently affected by the film morphology, such as grain sizes, roughness, and crystallinity. This is problematic especially when we compare the impedances of the interfaces with different electrode materials or different surface modifications, because they often alter the morphology of the electrode surface and that of the organic thin film. In order to separate the effect of the morphology on the measured impedance, it is important to measure the local impedance with an electrode smaller than the grain size.

Atomic force microscopy (AFM) is a very useful technique not only to image the morphology of the sample at a nanometer-scale resolution but also to investigate various local electrical properties, such as the potential difference between organic grains,[19] potential distribution of the

a)Electronic mail: h-yamada@kuee.kyoto-u.ac.jp.

operating OFETs,[4] and current–voltage characteristics of a single organic grain.[20,21] Among them, scanning impedance microscopy (SIM), which was developed by Kalinin and Bonnell,[22] can obtain information on the electrical impedance of an interface by laterally applying an ac modulation voltage to the interface of a sample and measuring the amplitude and phase of the electrostatic force between the tip and sample. They demonstrated the measurements of the local impedances of the grain boundaries of an inorganic semiconductor[22] and the metal-semiconductor Schottky junction.[23] Moreover, it has also been shown that SIM can be useful to identify the local defects in carbon nanotube networks.[24]

We now propose frequency-modulation SIM (FM-SIM), a technique based on the same concept as the original SIM, but modified in several aspects as described below. First, we utilized the FM technique[25] not only because it allows us to operate SIM in a vacuum, which is essential for the electrical measurement of the OFETs, with a realistic measurement time but also because the electrostatic force between the tip and sample can be detected with a lateral resolution higher than that by the amplitude-modulation method used in the original SIM.[26] In the original SIM, the dc potential drop across the interface should be separately measured by a surface potential measurement technique, Kelvin-probe force microscopy (KFM),[27,28] and its effect on the SIM signal should be taken into account to interpret the SIM measurement results. In the FM-SIM technique that we developed, the FM-KFM is implemented at the same time; namely, the dc potential drop across the interface and the electrical impedance can be simultaneously measured in a single measurement. In this study, we measured the local impedance of a single pentacene grain connected to a single electrode by FM-SIM, which is regarded as a simple metal–organic interface model of the bottom-contact OFETs and the laterally connected metal-insulator-semiconductor structure usually used in capacitance-voltage measurements, and we discuss the relationship between the contact resistance and the electronic properties at the metal–grain interface.

II. PRINCIPLE OF FM-SIM

Figure 1 shows a schematic diagram of the FM-SIM measurement setup for measuring the local impedance of the interface between an electrode and an organic grain. In FM-SIM, the local impedance is simultaneously measured along with the topography by the conventional frequency modulation atomic force microscopy (FM-AFM) and surface potential by FM-KFM. The cantilever is self-oscillated at its resonance frequency (f_0) using a self-excitation circuit (not drawn in the figure), and the distance between the cantilever tip and sample is regulated by keeping the dc component in the frequency shift (Δf^{dc}) of the cantilever constant, enabling the topographic imaging in the constant frequency shift mode (FM-AFM). A bias voltage is applied to the tip, $V_{\mathrm{t}} = V_{\mathrm{t}}^{\mathrm{dc}} + V_{\mathrm{t}}^{\mathrm{ac}} \cos 2\pi f_{\mathrm{t}} t$, where $V_{\mathrm{t}}^{\mathrm{dc}}$ is a dc control voltage that compensates the contact potential difference between the tip and the local area of the sample under the tip (FM-KFM). At the same time, another bias voltage is applied to the electrode of the sample ($V_{\mathrm{s}} = V_{\mathrm{s}}^{\mathrm{dc}} + V_{\mathrm{s}}^{\mathrm{dc}} \cos 2\pi f_{\mathrm{s}} t$). If

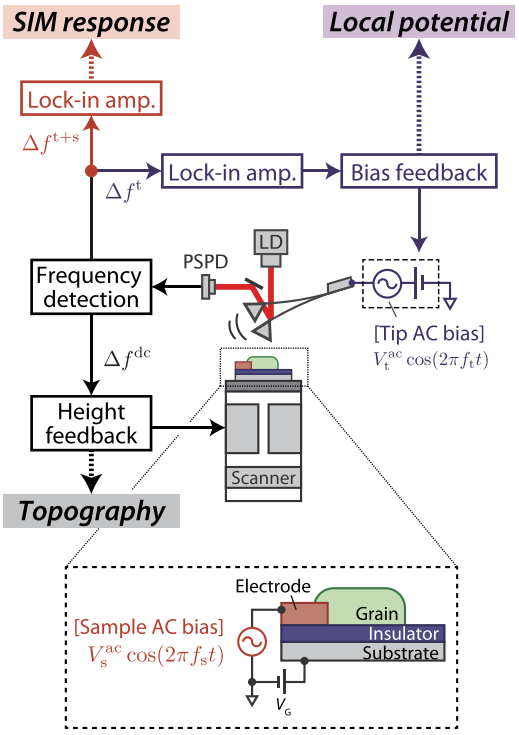

FIG. 1. Schematic diagram of the FM-SIM measurement setup. The conductive cantilever is oscillated at its resonance frequency, and the topography is obtained by scanning the tip over the sample while the tip-sample distance is regulated by keeping the dc component of the frequency shift (Δf^{dc}) constant (FM-AFM). Two ac bias voltages are applied to the cantilever (frequency: f_{t}, amplitude: $V_{\mathrm{t}}^{\mathrm{ac}}$) and to the electrode ($f_{\mathrm{s}}$, $V_{\mathrm{s}}^{\mathrm{ac}}$). The resonance frequency shift (Δf) is modulated at f_{t} (Δf^{t}), and the local electrical potential is measured by detecting the f_{t} component in Δf. At the same time, the $f_{\mathrm{s}} + f_{\mathrm{t}}$ component in Δf ($\Delta f^{\mathrm{t+s}}$) is also detected as the FM-SIM signal.

we describe the electrical potential of the local area as $V_{\mathrm{lo}} = V_{\mathrm{lo}}^{\mathrm{dc}} + V_{\mathrm{lo}}^{\mathrm{ac}} \cos(2\pi f_{\mathrm{s}} t + \phi_{\mathrm{lo}})$, the electrostatic force exerted on the cantilever tip is given by

$$F_{\mathrm{ES}} = \frac{1}{2}\frac{\partial C_{\mathrm{ts}}}{\partial z}\left[V_{\mathrm{lo}}^{\mathrm{dc}} + V_{\mathrm{t}}^{\mathrm{dc}} + V_{\mathrm{t}}^{\mathrm{ac}} \cos 2\pi f_{\mathrm{t}} t + V_{\mathrm{lo}}^{\mathrm{ac}} \cos(2\pi f_{\mathrm{s}} t + \phi_{\mathrm{lo}})\right]^2, \quad (1)$$

where z and C_{ts} are the distance and capacitance between the tip and the sample, respectively. There are several frequency components in F_{ES}, among which a component at f_{t} is given by

$$F_{\mathrm{ES}}^{\mathrm{t}} = \frac{\partial C_{\mathrm{ts}}}{\partial z}\left(V_{\mathrm{lo}}^{\mathrm{dc}} + V_{\mathrm{t}}^{\mathrm{dc}}\right) V_{\mathrm{t}}^{\mathrm{ac}} \cos 2\pi f_{\mathrm{t}} t. \quad (2)$$

The frequency modulation induced by $F_{\mathrm{ES}}^{\mathrm{t}}$, denoted as Δf^{t}, is detected by a lock-in amplifier (LIA). The output of the LIA is then fed to a bias feedback circuit to generate a dc control voltage ($V_{\mathrm{t}}^{\mathrm{dc}}$) that compensates the contact potential difference between the tip and the local area of the sample under the tip and nullifies $F_{\mathrm{ES}}^{\mathrm{t}}$. This enables the measurement of the local dc potential ($V_{\mathrm{lo}}^{\mathrm{dc}}$) by FM-KFM. The frequency component at $f_{\mathrm{s}} \pm f_{\mathrm{t}}$ in F_{ES}, given by

$$F_{\mathrm{ES}}^{\mathrm{t}\pm\mathrm{s}} = \frac{1}{2}\frac{\partial C_{\mathrm{ts}}}{\partial z} V_{\mathrm{t}}^{\mathrm{ac}} V_{\mathrm{lo}}^{\mathrm{ac}} \cos[2\pi(f_{\mathrm{t}} \pm f_{\mathrm{s}})t \pm \phi_{\mathrm{lo}}], \quad (3)$$

also induces the frequency modulation in the resonance frequency of the cantilever, which is denoted as $\Delta f^{t\pm s}$. The magnitude of $\Delta f^{t\pm s}$ is proportional to the potential modulation (V_{lo}^{ac}) of the local area under the tip, and the phase of $\Delta f^{t\pm s}$ is exactly the same as that of the potential modulation (ϕ_{lo}). The phasor representation of the sum frequency component, given by $\Delta\tilde{f}^{t+s} = \alpha {V_{lo}}^{ac} e^{j\phi_{lo}}$, is defined as the "FM-SIM signal." α is a proportional factor that is constant during a single measurement as long as the tip–sample distance and the mechanical oscillation amplitude of the cantilever at $f_0 + \Delta f^{dc}$ remain constant.

The measured FM-SIM signal can be easily converted to the local impedance of the metal–grain interface (Z_{lo}). Figure 2(a) shows an equivalent circuit of the measured interface with the effective capacitance of the insulator under the organic grain (C_i). It is assumed that the impedance of the grain is much smaller than that of the interface, and the potential of the grain is uniformly constant at V_{lo}. The validity of this assumption is discussed later. As the FM-SIM signal measured when the tip is on the electrode is given by αV_s^{ac}, we define the "normalized FM-SIM signal" (γ) as

$$\gamma = \frac{\alpha V_{lo}^{ac} e^{j\phi_{lo}}}{\alpha V_s^{ac}}. \tag{4}$$

It is also related to the complex voltage division ratio by the impedances of the interface and that of the effective capacitance as

$$\gamma = \frac{1/(j2\pi f_s C_i)}{Z_{lo} + 1/(j2\pi f_s C_i)} = \frac{1}{1 + j2\pi f_s C_i Z_{lo}}. \tag{5}$$

Therefore, we can estimate Z_{lo} by measuring γ on the grain (FM-SIM).

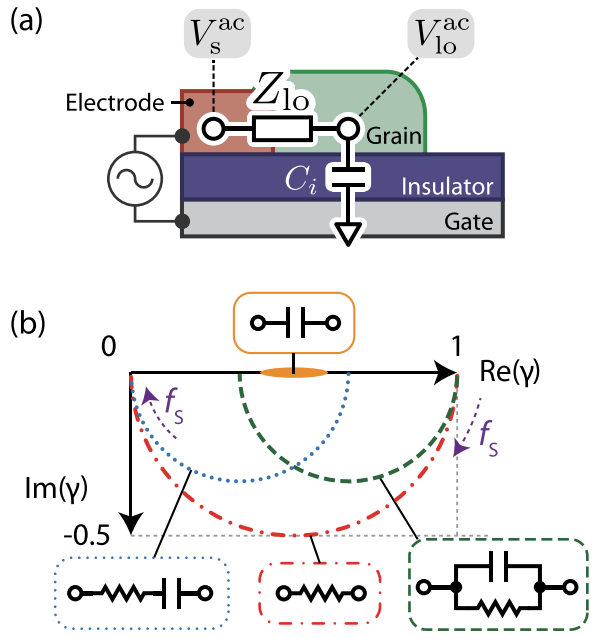

FIG. 2. (a) Schematic illustration of the sample structure and equivalent circuit. Z_{lo} is the interface impedance between the electrode and grain, and C_i is the effective insulator capacitance under the grain. (b) Theoretical plots of the normalized FM-SIM signals (γ) for Z_{lo} modeled with various equivalent circuits.

If we measure γ as a function of f_s and plot it in the complex plane, we can determine the appropriate equivalent circuit model. Figure 2(b) shows the theoretical plots of γ for various equivalent circuit models. If Z_{lo} is resistive, γ follows a semicircle with a diameter of unity. On the other hand, if Z_{lo} is capacitive, γ stays on the real axis. If Z_{lo} is modeled as a series or parallel circuit of the resistor and capacitance (RC-series or RC-parallel), γ gives a semicircle with a diameter of less than unity starting at 1 or ending at 0, respectively, as shown in Fig. 2(b).

III. MATERIAL AND METHODS

A. Sample preparation

We fabricated pentacene thin films connected to a Pt electrode for the local impedance measurement of the metal–grain interface. The pentacene molecule is a π-conjugated p-type semiconductor whose fundamental electrical properties have been intensively studied.[29] We fabricated a Pt electrode whose thickness and width were approximately 10 nm and 100 nm, respectively, by electron beam lithography on a highly doped n-type Si substrate (dopant: Sb, resistivity: $\leq$0.02 Ω cm) with a 100-nm-thickness thermally grown oxide layer. After UV/ozone cleaning of the substrate for 30 min, we deposited the pentacene molecules with an average thickness of 17 nm by vapor deposition while the substrate temperature was kept at 30 °C.

B. FM-SIM measurement

We used a commercially available AFM apparatus (JEOL: JSPM-4200) with a lab-built AFM controller. We used a Pt-coated conductive cantilever (Olympus: OMCL-AC240TM-R3), whose nominal spring constant and resonance frequency were 2 N/m and 70 kHz, respectively. The cantilever was mechanically oscillated at f_0 and the oscillation amplitude was kept at about 15 $nm_{p\text{-}p}$. The frequency shift was detected by a lab-built FM detector,[30] and the frequency modulation components were demodulated by lock-in amplifiers (NF Corporation: LI5640 and Zurich Instruments: HF2LI-MF). We always set f_t and V_t^{ac} at 1 kHz and 2 $V_{p\text{-}p}$, respectively, while the parameters of the bias voltage applied to the electrode varied depending on the experiments. All of the measurements were performed at room temperature and under a vacuum condition ($<1 \times 10^{-3}$ Pa) in order to reduce the effects of atmospheric oxygen and water.

IV. RESULTS AND DISCUSSION

An FM-AFM topographic image of the obtained pentacene film is shown in Fig. 3. The surfaces of the pentacene grains are partially flat but exhibit step and terrace structures with a step height of about 1.7 nm, indicating that the long axis of the pentacene molecules is almost perpendicular to the substrate as already reported.[31] We found that a grain "A" indicated by the white arrow in the figure was obviously isolated from the other grains and directly connected to the Pt electrode. Therefore, the interface between the Pt electrode and grain A is well described by the equivalent circuit,

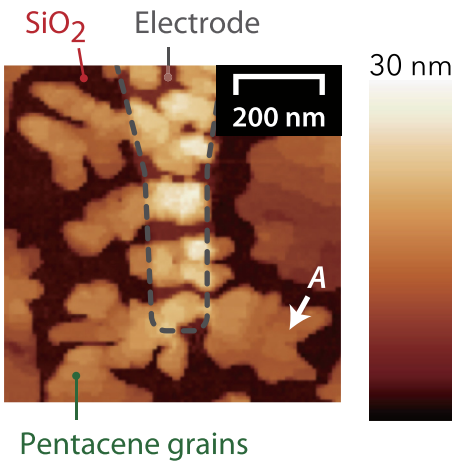

FIG. 3. Topographic image of pentacene grains near the metal electrode, which is enclosed by the dashed curve. The dark area surrounding the electrode and grains is the bare SiO_2 surface. Grain A indicated by the arrow is isolated from the other grains.

and we chose this interface as the target interface for the FM-SIM measurement.

We first performed the FM-SIM measurement at the interface between the Pt electrode and grain A by recording both the amplitude and phase of the FM-SIM signal, while the tip was raster-scanned over the sample surface and no gate bias voltage was applied ($V_G = 0$ V). Figures 4(a) and 4(b) show a topographic image and a surface potential image of the area of concern recorded during the FM-SIM measurement, respectively. Figures 4(c) and 4(d) show the amplitude and phase images of the FM-SIM signal, respectively, taken with $V_s^{ac} = 1$ $V_{p\text{-}p}$. We note here that the reference phase of the LIA was adjusted such that the phase of the FM-SIM signal on the electrode became zero. Figure 4(c) shows that the amplitude of the FM-SIM signal was almost uniform within grain A. It is also clear from Fig. 4(d) that the FM-SIM phase signal on grain A was also uniform, and there was a significant difference in the FM-SIM phase signal across the interface, while the other grains connected to the electrode showed the phase signal close to the electrode. In this case, the FM-SIM images suggest two aspects: the grain A was not electrically well-coupled and the local impedance of the pentacene grain is much smaller than that of the metal–grain interface. The FM-SIM images often allow us to locate the sites with significant electrical impedance, considering the principle of the FM-SIM. Figures 4(e) and 4(f) show the topography and the FM-SIM phase image, respectively, of a large area near the electrodes at $V_G = -2$ V. We found that the pentacene grains showed a variety of the phase signal in a range between $-40°$ and $0°$, which is the phase on the electrode. The heterogeneity in the phase signal on the grains indicates the differences in the local impedance at each metal–grain interface. However, the positive or negative phase shift compared to the electrode does not directly correlate with a good or poor electrical coupling. We have to convert the FM-SIM signals to evaluate the impedance to discuss on the electrical coupling. Hereinafter, we will discuss the FM-SIM measurement results using the equivalent circuit models shown in Fig. 2.

Second, we measured the normalized FM-SIM signal on grain A as a function of f_s to determine the equivalent circuit of the interface with $V_s^{ac} = 1$ $V_{p\text{-}p}$. In this measurement, we set V_G to -5 V such that the pentacene grains were in the hole accumulation regime. We recorded the FM-SIM signals on grain A and the electrode at f_s ranging from 10 Hz to 900 Hz. The normalized FM-SIM signal (γ) calculated using Eq. (4) was plotted on the complex plane in Fig. 5. We found that the measured γ at low frequencies was close to 1, and it followed a semicircle with a diameter smaller than 1 as f_s increased; namely, the interface impedance is well depicted by the RC-parallel in Fig. 2(b). The impedance of the RC-parallel circuit is given by $Z_{lo} = (R_{lo}^{-1} + j2\pi f_s C_{lo})^{-1}$; however, if the interface impedance is represented by the

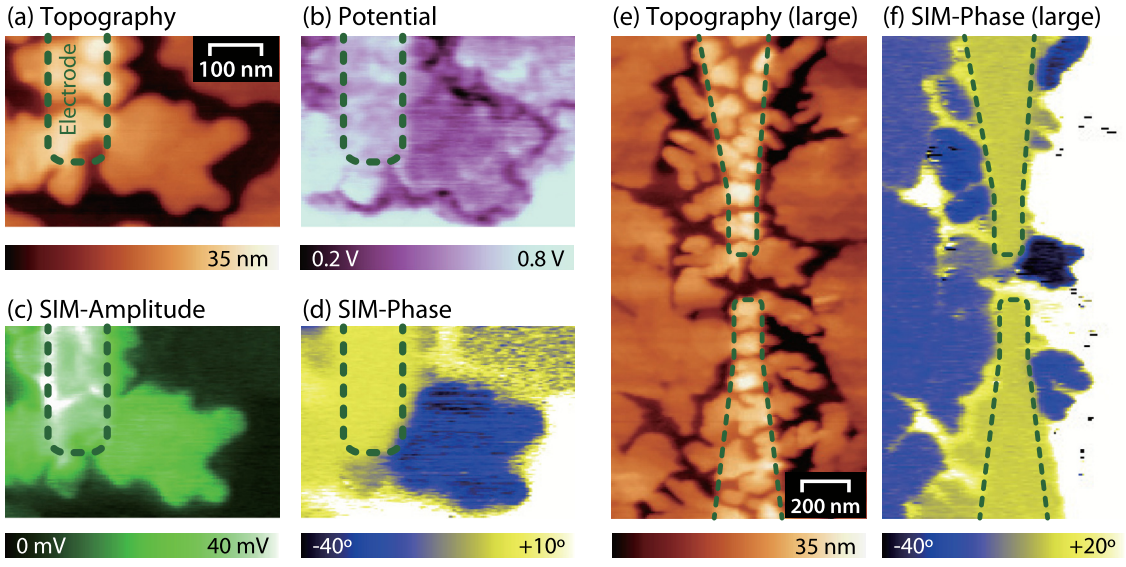

FIG. 4. (a) Topographic, (b) surface potential, (c) amplitude FM-SIM, and (d) phase FM-SIM images of the area around the interface between the Pt electrode and grain A measured at $V_G = 0$ V. While the amplitude of the FM-SIM signal on grain A was almost as uniform as that on the electrode, a distinct difference was observed in the FM-SIM phase signal across the interface in (d). (e) and (f) Topographic and FM-SIM phase images, respectively, of a large area near the Pt electrodes measured at $V_G = -2$ V.

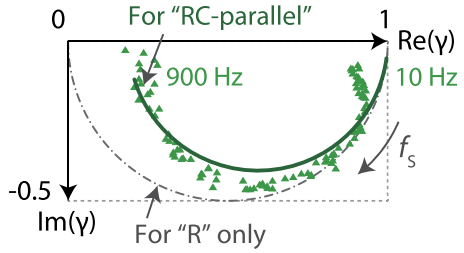

FIG. 5. Plot of the normalized FM-SIM signal (γ) measured at the interface between the electrode and grain A. The solid curve shows the theoretical γ curve for the parallel circuit of a resistance and a capacitance (RC-parallel) that gave the best fit to the experimental result.

RC-parallel circuit, it is more intuitive to discuss in terms of the admittance rather than the impedance, $Y_{lo} = Z_{lo}^{-1} = R_{lo}^{-1} + j2\pi f_s C_{lo}$. In the following, we use the admittance (conductance and susceptance) to discuss the interface between the grain A and the electrode instead of the impedance (resistance and reactance).

The normalized admittance, that is, the interface admittance normalized by the effective insulator susceptance was then introduced and given by

$$Y_{norm} = (R_{lo}^{-1} + j2\pi f_s C_{lo})/2\pi f_s C_i = 1/2\pi f_s C_i R_{lo} + j(C_{lo}/C_i), \quad (6)$$

which can be calculated from γ as $Y_{norm} = j\gamma/(1-\gamma)$. We fitted the theoretical γ curve to the experimental γ curve and found that the curve with the parameters $C_i R_{lo} = 0.84$ ms and $C_{lo}/C_i = 0.23$ gave the best fit to the result, as shown by the solid curve in Fig. 5. This result pointed out the existence of a local capacitance at the metal–organic interface and a contact resistance. Previous reports ascribed the interface capacitance to the energy mismatch between E_F and E_{HOMO}.[17,32] However, these reports studied the top-contact OFETs, where the organic films were sandwiched between the electrodes and the gate insulator. Since the thickness of the organic film is typically thicker than the conducting channel where the carriers are accumulated, the measured impedance for the top-contact OFETs might include not only the intrinsic metal-organic interface but also the impedance of the bulk region in the organic film above the channel. However, as our experiments were performed on bottom-contact organic thin films, the existence of the capacitive component in the metal-organic interface admittance (or impedance) was more directly revealed by the FM-SIM than the previous reports.

These FM-SIM measurements were performed when the carriers were accumulated in the pentacene grain, that is, in the hole accumulation regime. However, the electronic properties at the metal–organic interface should change according to the degree of the carrier accumulation in the grain. In order to clarify the origin of the metal–organic contact resistance, we investigated the change in the interface admittance as a function of V_G. We fixed f_S at 100 Hz and recorded the FM-SIM signals while the tip was scanned along the A-B line indicated in a topographic image shown in Fig. 6(a). V_G was changed from +2 V to −3 V (forward) and then reverted to +2 V (backward). V_s^{ac} was set to 0.2 $V_{p\text{-}p}$ in this case to

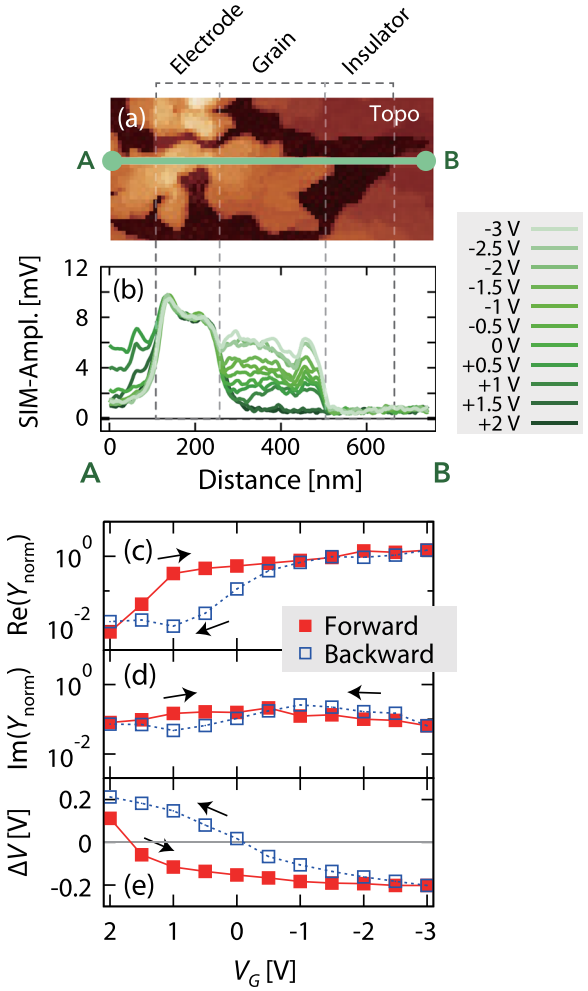

FIG. 6. (a) Topographic FM-AFM image of the area around the interface between the Pt electrode and grain A. (b) FM-SIM amplitude signal profiles measured along the A-B line indicated in (a). (c) and (d) The plots of the real part and imaginary part of the normalized interface admittance Y_{norm} as a function of V_G, respectively. (e) The plot of the potential drop across the interface ΔV as a function of V_G. The solid symbols represent the data points measured during the forward sweep of V_G from +2 V to −3 V, and the open symbols represent the data points during the backward sweep.

minimize the averaging effect because V_G and V_s^{ac} are in series (see Fig. 1). Figure 6(b) shows the FM-SIM amplitude signal profiles measured at V_G from +2 V to −3V (forward) along the A-B line indicated in Fig. 6(a). The FM phase signal profiles are also available in the supplementary material.[33] While the magnitude of the FM-SIM amplitude signal on the electrode stayed constant as expected, those on the grains gradually changed. We averaged the FM-SIM amplitude and phase signals on the electrode and grain A, and calculated the normalized FM-SIM signal (γ) and then the normalized admittance of the interface (Y_{norm}). In order to discuss the dependence of the admittance as a function of the voltage drop at the interface, we plotted the real and imaginary components of the normalized interface admittance as well as the voltage drop across the interface (ΔV) measured from the surface potential profiles simultaneously recorded by FM-KFM with FM-SIM (Figs. 6(c)–6(e)).

We found that the conductance (real part of Y_{norm}) drastically increased as a more negative V_G was applied, while

the interface susceptance (imaginary part of Y_{norm}) did not show an obvious change. The reduction of the contact resistance as V_G increases is often seen in previous studies on the OFETs.[9,10,34] Several models were suggested for the reasons of the contact resistance reduction induced by V_G, such as the effect of the bulk organic layer and the low mobility region near the electrode.[34,35] However, these explanations are valid for the top-contact electrode or the OFETs with multi-grain films. As our FM-SIM measurements presented here were performed for the interface of the metal and single organic grain with the bottom-contact structure, we can rule out the effects of both the bulk layer and the grain boundary interfaces on the measured admittance (or impedance). Therefore, the increase in the conductance (or reduction of the contact resistance) by applying a negative V_G that we observed here reflects the intrinsic property of the injection barrier at the metal–grain interface, of which the previous studies cannot directly access.

It is of significant importance that the interface conductance in Fig. 6(c) and ΔV in Fig. 6(e) showed a similar hysteretic behavior between the forward and backward V_G sweeps. A similar hysteretic behavior is often found in the transfer characteristics of the OFETs.[36] The accumulation of holes is accompanied by hole trapping in deep trap states at the organic–insulator interface, which shifts the necessary V_G for making the channel conductive, that is, the threshold voltage to a negative value in the backward sweep. The hysteretic behavior observed here can also be attributed to the deep trap states at the organic–insulator interface, because SiO_2, the insulator we used, tends to cause significant hysteresis in the OFET characteristics. Generally, the interface capacitance is determined by fast charge/discharge of the mobile carriers and slow charge/discharge of the deeply trapped carriers at the interface, which cause the hysteretic behavior. While the latter may vary depending on the charge accumulation, the former is considered as constant. As the FM-SIM measures the ac responses of the interface to an ac voltage applied across the interface, the FM-SIM measures the former in principle. Therefore, the deeply trapped holes at the organic–insulator interface do not change the effective C_i measured by the FM-SIM, and only a small variation was observed for the interface capacitance (Fig. 6(d)).

A plot of the interface conductance as a function of ΔV (Fig. 7(a)), which shows less hysteresis between both sweeps, indicates that the metal–grain interface properties is determined not by V_G itself but by the interfacial potential drop ΔV. Therefore, the observed hysteretic behaviors of the conductance and the potential drop are not intrinsic properties of the metal–organic interface. From Fig. 7(a), it was determined that there was almost no interface conductance $\mathrm{Re}(Y_{norm})$ at $\Delta V > 0$ V, while the interface conductance increased at $\Delta V < 0$ V, corresponding to the hole depletion and accumulation regime induced by the positive and negative V_G. The interface conductance showed a steep increase roughly at $\Delta V = -0.2$ V, which indicates that the interfacial voltage drop of -0.2 V was needed for the metal–grain interface to become conductive. The change in the metal–organic interface conductance can be explained by the following description. Figures 7(b) and 7(c) illustrate energy diagrams of the metal–organic interface between the Pt electrode and the pentacene grain. In the zero-bias condition, E_F is located higher than E_{HOMO}, which produces the hole injection barrier, and the pentacene film is in the hole depletion regime (Fig. 7(b)). There is a significant energy mismatch between the E_F and E_{HOMO} of the organic grain. In this situation, a high energy is needed for a hole to be injected from the electrode into the organic grain, and it appears as a high contact resistance. Note that the carrier accumulation layer at the organic–insulator interface has a non-zero density of trap states in the energy gap between E_{HOMO} and E_{LUMO}, the energy of the lowest unoccupied molecular orbital (LUMO) level. These states are partly filled even at the zero-bias condition, which fix E_F between E_{HOMO} and E_{LUMO}.

When a negative V_G is applied to the gate electrode, more trap states are filled and E_F approaches E_{HOMO}, which induces a negative ΔV. The energy mismatch becomes low, allowing the holes to be easily injected into the grain, which leads to a lower contact resistance (the hole accumulation regime), as shown in Fig. 7(b). Thus, the application of V_G produced a change in the energy alignment condition at the metal–organic interface. While this simple interpretation has already been discussed on the basis of the electrical measurements using electrodes having various work functions or

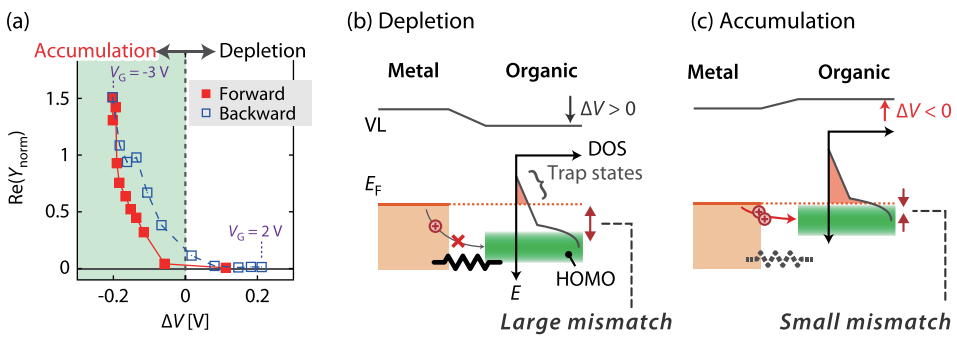

FIG. 7. (a) Plot of the interface conductance $\mathrm{Re}(Y_{norm})$ as a function of the voltage drop during the forward ($V_G = +2$ V to -3 V, solid symbols) and backward (-3 V to $+2$ V, open symbols) sweeps. (b) and (c) Energy diagrams of the metal–organic interface between the Pt electrode and the pentacene grain. The density of states (DOS) vs. hole energy (E) in the organic grain is also depicted in each diagram. (b) When the voltage drop across the interface is positive ($\Delta V > 0$), the hole injection is inhibited by a significant energy mismatch between E_F and E_{HOMO}. The trap states above the HOMO level are partly filled as depicted in the DOS-E diagram. (c) For $\Delta V < 0$, the holes are accumulated in the organic grain, and more trap states are filled as depicted in the DOS-E diagram, which leads to a low energy mismatch that reduces the contact resistance.

SAMs having different electrical dipoles, it is remarkable that the relationship between the energy alignment condition and the contact resistance can be discussed on a single-grain scale by the FM-SIM measurement. The results demonstrate that one can use the FM-SIM technique as the local impedance measurement tool with an electrode smaller than the grain size, which enables us to measure the intrinsic impedance without being affected by the morphology of the interface.

V. CONCLUSIONS

We developed FM-SIM by combining FM-AFM and heterodyne electrostatic force sensing to investigate the local impedance at the interface between a metal electrode and a single grain as well as the potential drop at the interface. The measured interface impedance was well described by the equivalent circuit of a contact resistance and a capacitance in parallel. We found the contact resistance at the interface decreases upon application of negative gate bias voltages with a hysteretic behavior, which has also been previously reported. However, by simultaneously measuring the effective voltage drop at the interface, we concluded that the hysteretic behavior is not an intrinsic property of the contact resistance, but caused by the charge trapping at the organic–insulator interface, and we explained the reduction in the contact resistance in terms of the reduction in the energy mismatch, which hinders hole injection at the interface. These results demonstrated the usefulness of the FM-SIM technique for investigation of the intrinsic electronic properties of a metal–organic interface without being affected by the morphology of the interface, unlike the impedance measurements using macroscopic electrodes.

ACKNOWLEDGMENTS

This work was supported by Grants-in-Aid for Scientific Research from the Japan Society for the Promotion of Science.

[1]T. Sekitani and T. Someya, Adv. Mater. **22**, 2228 (2010).
[2]D. J. Gundlach, J. E. Royer, S. K. Park, S. Subramanian, O. D. Jurchescu, B. H. Hamadani, A. J. Moad, R. J. Kline, L. C. Teague, O. Kirillov, C. A. Richter, J. G. Kushmerick, L. J. Richter, S. R. Parkin, T. N. Jackson, and J. E. Anthony, Nature Mater. **7**, 216 (2008).
[3]D. J. Gundlach, L. Zhou, J. A. Nichols, T. N. Jackson, P. V. Necliudov, and M. S. Shur, J. Appl. Phys. **100**, 024509 (2006).
[4]K. P. Puntambekar, P. V. Pesavento, and C. D. Frisbie, Appl. Phys. Lett. **83**, 5539 (2003).
[5]H. Minemawari, T. Yamada, H. Matsui, J. Tsutsumi, S. Haas, R. Chiba, R. Kumai, and T. Hasegawa, Nature **475**, 364 (2011).
[6]A. Valletta, A. Daami, M. Benwadih, R. Coppard, G. Fortunato, M. Rapisarda, F. Torricelli, and L. Mariucci, Appl. Phys. Lett. **99**, 233309 (2011).
[7]M. Rapisarda, A. Valletta, A. Daami, S. Jacob, M. Benwadih, R. Coppard, G. Fortunato, and L. Mariucci, Org. Electron. **13**, 2017 (2012).
[8]P. V. Pesavento, R. J. Chesterfield, C. R. Newman, and C. D. Frisbie, J. Appl. Phys. **96**, 7312 (2004).
[9]S. D. Wang, T. Minari, T. Miyadera, K. Tsukagoshi, and Y. Aoyagi, Appl. Phys. Lett. **91**, 203508 (2007).
[10]C. Reese and Z. Bao, Adv. Funct. Mater. **19**, 763 (2009).
[11]L. Bürgi, T. J. Richards, R. H. Friend, and H. Sirringhaus, J. Appl. Phys. **94**, 6129 (2003).
[12]P. Marmont, N. Battaglini, P. Lang, G. Horowitz, J. Hwang, A. Kahn, C. Amato, and P. Calas, Org. Electron. **9**, 419 (2008).
[13]J.-P. Hong, A.-Y. Park, S. Lee, J. Kang, N. Shin, and D. Y. Yoon, Appl. Phys. Lett. **92**, 143311 (2008).
[14]P. Darmawan, T. Minari, A. Kumatani, Y. Li, C. Liu, and K. Tsukagoshi, Appl. Phys. Lett. **100**, 013303 (2012).
[15]S. D. Wang, T. Miyadera, T. Minari, Y. Aoyagi, and K. Tsukagoshi, Appl. Phys. Lett. **93**, 043311 (2008).
[16]J. Zaumseil, K. W. Baldwin, and J. A. Rogers, J. Appl. Phys. **93**, 6117 (2003).
[17]T. Miyadera, T. Minari, K. Tsukagoshi, H. Ito, and Y. Aoyagi, Appl. Phys. Lett. **91**, 013512 (2007).
[18]S. Karg, W. Riess, V. Dyakonov, and M. Schwoerer, Synth. Met. **54**, 427 (1993).
[19]M. Nakamura, H. Ohguri, N. Goto, H. Tomii, M. Xu, T. Miyamoto, R. Matsubara, N. Ohashi, M. Sakai, and K. Kudo, Appl. Phys. A **95**, 73 (2009).
[20]T. Kimura, Y. Miyato, K. Kobayashi, H. Yamada, and K. Matsushige, Jpn. J. Appl. Phys., Part 1 **51**, 08KB05 (2012).
[21]M. Hirose, E. Tsunemi, K. Kobayashi, H. Yamada, and K. Matsushige, Jpn. J. Appl. Phys. **49**, 08LB10 (2010).
[22]S. V. Kalinin and D. A. Bonnell, Appl. Phys. Lett. **78**, 1306 (2001).
[23]S. V. Kalinin and D. A. Bonnell, J. Appl. Phys. **91**, 832 (2002).
[24]S. V. Kalinin, S. Jesse, J. Shin, A. P. Baddorf, M. A. Guillorn, and D. B. Geohegan, Nanotechnology **15**, 907 (2004).
[25]T. Albrecht, P. Grutter, D. Horne, and D. Rugar, J. Appl. Phys. **69**, 668 (1991).
[26]U. Zerweck, C. Loppacher, T. Otto, S. Grafström, and L. Eng, Phys. Rev. B **71**, 125424 (2005).
[27]J. Weaver and D. W. Abraham, J. Vac. Sci. Technol. B **9**, 1559 (1991).
[28]M. Nonnenmacher, M. P. O'Boyle, and H. K. Wickramasinghe, Appl. Phys. Lett. **58**, 2921 (1991).
[29]G. Horowitz, J. Mater. Res. **19**, 1946 (2004).
[30]K. Kobayashi, H. Yamada, H. Itoh, T. Horiuchi, and K. Matsushige, Rev. Sci. Instrum. **72**, 4383 (2001).
[31]R. Mishima, N. T. Loan, and H. Tada, Jpn. J. Appl. Phys., Part 1 **51**, 045702 (2012).
[32]M. Kano, T. Minari, and K. Tsukagoshi, Appl. Phys. Lett. **94**, 143304 (2009).
[33]See supplementary material at http://dx.doi.org/10.1063/1.4927921 for the FM-SIM phase signal profiles.
[34]T. Minari, T. Miyadera, K. Tsukagoshi, Y. Aoyagi, and H. Ito, Appl. Phys. Lett. **91**, 053508 (2007).
[35]T. Minari, P. Darmawan, C. Liu, Y. Li, Y. Xu, and K. Tsukagoshi, Appl. Phys. Lett. **100**, 093303 (2012).
[36]M.-H. Yoon, C. Kim, A. Facchetti, and T. J. Marks, J. Am. Chem. Soc. **128**, 12851 (2006).